Available online at www.sciencedirect.com
SCIENCE DIRECT®
Chaos, Solitons and Fractals 24 (2005) 645–652
CHAOS SOLITONS & FRACTALS
www.elsevier.com/locate/chaos

Direct characterization of chaotic and stochastic dynamics in a population model with strong periodicity

Wen-wen Tung [a], Yan Qi [b], J.B. Gao [c,*], Yinhe Cao [d], Lora Billings [e]

[a] National Center for Atmospheric Research, Boulder, CO 80307-3000, USA
[b] Department of Biomedical Engineering, Johns Hopkins University, Baltimore, MD 21205, USA
[c] Department of Electrical and Computer Engineering, University of Florida, Gainesville, FL 32611, USA
[d] BioSieve, 1026 Springfield Drive, Campbell, CA 95008, USA
[e] Department of Mathematical Sciences, Montclair State University, Montclair, NJ 07043, USA

Accepted 15 September 2004

Abstract

In recent years it has been increasingly recognized that noise and determinism may have comparable but different influences on population dynamics. However, no simple analysis methods have been introduced into ecology which can readily characterize those impacts. In this paper, we study a population model with strong periodicity and both with and without noise. The noise-free model generates both quasi-periodic and chaotic dynamics for certain parameter values. Due to the strong periodicity, however, the generated chaotic dynamics have not been satisfactorily described. The dynamics becomes even more complicated when there is noise. Characterizing the chaotic and stochastic dynamics in this model thus represents a challenging problem. Here we show how the chaotic dynamics can be readily characterized by the direct dynamical test for deterministic chaos developed by [Gao JB, Zheng ZM. Europhys. Lett. 1994;25:485] and how the influence of noise on quasi-periodic motions can be characterized as asymmetric diffusions wandering along the quasi-periodic orbit. It is hoped that the introduced methods will be useful in studying other population models as well as population time series obtained both in field and laboratory experiments.

1. Introduction

Time series of population fluctuations are often complicated. In recent years it has been realized that this complexity may arise from the interplay of noise, forcing, and non-linear dynamics [1]. In order to assess the relative impacts of each factor, one has to first understand the characteristic features that each aspect may generate. A crucial step for achieving this goal is to be able to reliably distinguish between the effects on the dynamics due to noise and due to intrinsic non-linearity, especially chaos. However, no analysis method even partially capable of this has been introduced into population ecology. In fact, Hastings et al. [2] have pointed out that based on the primitive definition of sensitive dependence on initial conditions from chaos theory, there is no dichotomy between stochasticity and chaos. Such

* Corresponding author.
E-mail address: gao@ece.ufl.edu (J.B. Gao).

0960-0779/$ - see front matter © 2004 Elsevier Ltd. All rights reserved.
doi:10.1016/j.chaos.2004.09.076

behavior was also observed by Rand and Wilson [3] and motivated them to invent a new term "chaotic stochasticity". Actually a much less challenging problem of distinguishing between the motion on a torus (i.e., quasi-periodic motions) and chaotic motions have proven to be highly non-trivial and controversial [4,5]. To help gain deeper insights into the interplay of noise and intrinsic non-linearity, in this paper, we show, by studying a complicated noisy population model [6,7], how one may readily distinguish between quasi-periodic and chaotic motions, and how the effects of stochasticity can be conveniently characterized. The population model studied here has a strong global periodicity, and thus has eluded successful characterization of the small-scale chaotic motions in the model [6,8,9]. The behavior of the model becomes even more complicated when it contains intrinsic noise. However, the methods adopted in this paper successfully and fully characterize the rich behavior of the model dynamics.

The rest of the paper is organized as follows. In Section 2, we briefly describe the model and explain which aspects of the model behavior we shall study. In Section 3 we study how to distinguish between quasi-periodic and chaotic motions, and in Section 4 we study diffusions on the torus due to stochasticity. Section 5 contains concluding remarks.

2. Density-dependent two age-class model

Following Barahona and Poon [7], we study a noisy density-dependent two age-class model:

$$\begin{aligned} x_k &= r y_{k-1} \mathrm{e}^{-0.001(y_{k-1}+x_{k-1})} + \eta_x(n-1), \\ y_k &= 0.2 x_{k-1} \mathrm{e}^{-0.07(y_{k-1}+x_{k-1})} + 0.8 y_{k-1} \mathrm{e}^{y_{k-1}+0.5x_{k-1}} + \eta_y(n-1), \end{aligned} \tag{1}$$

where r is a parameter and η_x and η_y are white Gaussian noise terms with mean zero and standard deviation σ, uncorrelated to each other and to themselves. It is interesting to note that noise may affect virus spread in population dynamics [10].

Let us first consider the noise-free model. When $r = 117$, the motion is periodic. When $r = 118$, it is chaotic. The phase diagrams for these two cases are shown in Fig. 1(a) and (b), respectively. In either case, the motion has a strong global periodicity, as indicated by arrows in both figures. The global attractor is comprised of eight pieces. For

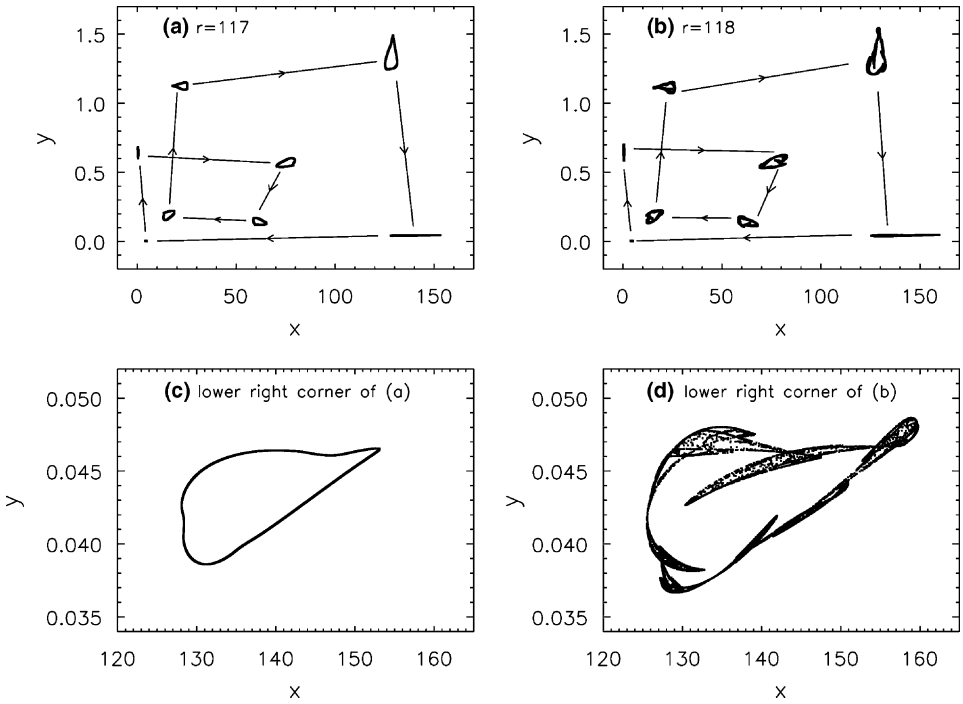

Fig. 1. Phase diagrams for (a) $r = 117$ and (b) $r = 118$. Arrows indicate the periodic transition from one part of the attractor to another. For simplicity, we call each such part an island. All together there are eight such islands. The islands located at the lower right corner of the figure are replotted in (c) and (d).

convenience, let us call each piece an island. To more clearly see what is going on within each island, in Fig. 1(c) and (d) we have re-plotted the lower right corner of Fig. 1(a) and (b). Now we clearly see that the island of Fig. 1(c) is periodic while that of Fig. 1(d) is chaotic. For later convenience, we denote the y-component of the original attractor by $\{y_n, n = 1, 2, \ldots\}$, and that of the lower right corner island by $\{y_n^{(R)},\ n = 1,\ 2,\ \ldots\}$. Note the sampling time for the former time series is simply 1, while that for the latter is 8.

To better appreciate the dynamics of the model at $r = 117$ and 118, in Fig. 2(a)–(d) we have plotted the power spectral density (PSD) for $\{y_n, n = 1, 2, \ldots\}$ and $\{y_n^{(R)},\ n = 1, 2, \ldots\}$ of Fig. 1(a)–(d). As expected, we observe a simple periodic spectrum in Fig. 2(c), corresponding to Fig. 1(c), and a broadband spectrum in Fig. 2(d), corresponding to Fig. 1(d). A broadband spectrum is often considered hallmark of chaos. Fig. 2(b), however, shows a few very sharp peaks superimposed on the background broadband spectrum. Those peaks are of course generated by the global periodic transitions between the eight chaotic islands. The fact that the periodic motion occurs on very large scale with very high power while chaos only occurs on very small scale with very low power makes characterization of such chaos from the global attractor very difficult [6,8,9]. The most interesting spectrum is that of Fig. 2(a). While one might be tempted to interpret that as a simple periodic spectrum with one basic frequency and lots of harmonics, it is actually a quasi-periodic spectrum with two basic frequencies. This can be readily understood if one notices that the motion is really on a (discrete) torus: one basic frequency is contributed by the periodic transitions between the eight islands, while another basic frequency describes the periodic motion inside each island. To better understand this, we can imagine that there are eight deformable continuous rotating rings jumping along a discrete orbit, with a total of eight jumps. Although it is not impossible to have different periodic motions within each island [11], it is not the case here. This, however, is more in line with the Ruelle and Takens quasi-periodic route to chaos [12].

Within the parameter range $117 \leqslant r \leqslant 118$, the dynamics of the model is very rich: the regular (mostly quasi-periodic) and chaotic motions are interspersed, and occasionally a quasi-periodic motion becomes simple periodic motion due to frequency-locking between the global periodic motion and the motion within each island. However, we do not study these bifurcations in detail here. Rather, we shall focus on how to distinguish between quasi-periodic and chaotic motions below. This has been considered to be more relevant to the analysis of population time series [4,5].

Next, we consider the noisy map. We have found that if the noise is too large, then the model diverges to infinity. Hence, we shall only consider weak noise. Amazingly, this global periodicity, both in the quasi-periodic and chaotic case, is preserved, even when there is noise. When the noise is weak, the shape of the attractor in Fig. 1(d) visually

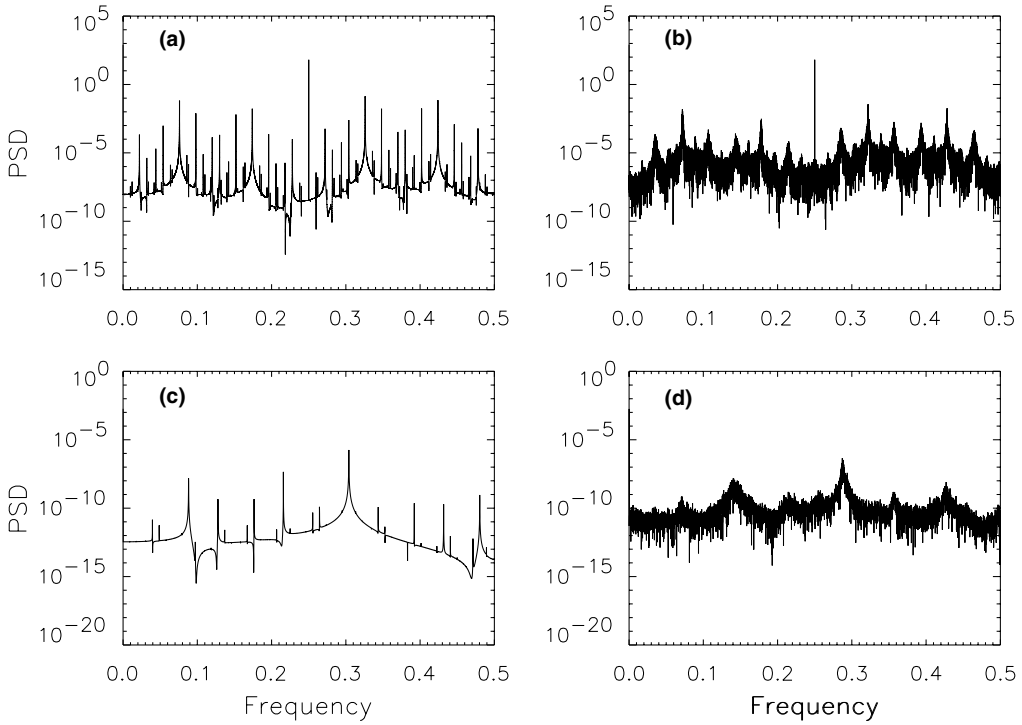

Fig. 2. (a)–(d) Power spectral density (PSD) for the time series of the y-component of Fig. 1(a)–(d).

remains more or less the same. However, that of Fig. 1(c) gets diffused out. In other words, the attractor is no longer a simple closed loop. Such diffused loops can often be mis-interpreted as chaos by unsophisticated chaos detection methods [2]. We shall show below that such diffused limit cycles can be conveniently described by a diffusional scaling law. That is, the distance between nearby orbits increases in a power-law manner, for large evolution time. This contrasts sharply with the exponential divergence in chaos, for fairly short evolution times.

Before we proceed on, we shall point out that the eight islands of the attractor are of very different size. In fact, the attractor located at the lower left corner is very much like a single point. While this is not really the case, as one may find out by enlarging that part, this nevertheless constitutes another dimension of difficulty in successfully characterizing the global attractor.

3. Characterization of the quasi-periodic and chaotic motions in the model

In order for the methods demonstrated in this paper to be directly applicable to the analysis of population time series, in this and next section, we shall be exclusively working with the y-component of the time series either from the global attractor or from one of the eight islands of the global attractor. Let us denote the scalar time series under consideration as $x(1), x(2), \ldots, x(N)$. For convenience, we shall first normalize the scalar time series into the unit interval $[0,1]$. We then use the time delay embedding procedure [13–15] to construct vectors of the form: $X_i = [x(i), x(i+L), \ldots, x(i+(m-1)L)]$, with m being the embedding dimension and L the delay time. We then compute a sequence of time-dependent exponent $\Lambda(k)$ curves, as defined by Gao and Zheng [16,17]:

$$\Lambda(k) = \left\langle \ln\left(\frac{\|X_{i+k} - X_{j+k}\|}{\|X_i - X_j\|}\right)\right\rangle \tag{2}$$

with $d \leqslant \|X_i - X_j\| \leqslant d + \Delta d$, where d and Δd are prescribed small distances. The angle brackets denote ensemble averages of all possible pairs of (X_i, X_j). The integer k, called the evolution time, corresponds to time $k\delta t$, where δt is the sampling time. Note that geometrically $(d, d+\Delta d)$ defines a shell, and a shell captures the notion of scale. The computation is carried out for a series of shells. The term $\|X_i - X_j\|$ can be thought of as the initial separation between two arbitrary orbits. The term $\|X_{i+k} - X_{j+k}\|$ then measures the separation between those two orbits after time $k\delta t$. For regular motions, with proper embedding parameters, all the $\Lambda(k)$ curves should be close to zero, since on the long run there is so separation between nearby orbits. For clean chaotic systems, the $\Lambda(k)$ curves first increase linearly with k till some predictable time scale, k_p, then flattens [18]. The linearly increasing parts of the $\Lambda(k)$ curves corresponding to different shells collapse together to form a common envelope, the slope of which estimates the largest positive Lyapunov exponent. This property forms a direct dynamical test for deterministic chaos [16,17], since the existence of the common envelope guarantees that a robust positive Lyapunov exponent will be obtained by different researchers no matter which shell they use in the computation, thus ensures determinism. For noisy chaotic systems, the linearly increasing parts of the $\Lambda(k)$ curves corresponding to small shells break themselves away from the envelope. The stronger the noise, the more the $\Lambda(k)$ curves break away from the envelope [19]. In short, when the dynamics is dominated by noise, then the common envelope is absent. Note that conventional methods for calculating the Lyapunov exponent, such as the one developed by Wolf et al. [20], amount to computing $\Lambda(k)$ for $d < d_0$, where d_0 is a small distance selected more or less arbitrarily, then obtaining $\Lambda(k)/k$, for not too large k, as an estimation of the largest Lyapunov exponent. So long as the size of the shells is small, $\Lambda(k)/k$ is positive. Because of this, many people then claim the time series under study is chaotic. However, when the common envelope is absent, then the estimated values for the largest Lyapunov exponent are not comparable among different researchers, since d_0 is arbitrary. This is a form of randomness!

Fig. 3 shows an example of the $\Lambda(k)$ curves for the $\{y_n^{(R)},\ n = 1, 2, \ldots\}$ of Fig. 1(c). Four different shells are used. The embedding parameters are $m = 4$ and $L = 1$. The computation is based on 1000 points. Clearly we observe that all the $\Lambda(k)$ curves are close to zero. While this feature is qualitatively always true for the regular cases we have considered here, we should point out that the exact "amplitude" of some of the $\Lambda(k)$ curves could be larger (up to 0.3) if one works on a short $\{y_n, n = 1, 2, \ldots\}$ time series of Fig. 1(a) and does not choose the embedding parameters carefully. This reflects the fact that the motion on the global attractor is not very uniform. This is readily understandable, since the sizes of the island can differ from one to another considerably. However, in any case, there is no danger of mis-interpreting the regular motion to be chaotic.

Next we consider the $\Lambda(k)$ curves for the chaotic time series. We first consider the simpler time series of $\{y_n^{(R)},\ n = 1, 2, \ldots\}$ of Fig. 1(d). The result is shown in Fig. 4(a), with $(m, L) = (4, 1)$. 2000 points are used in the computation. The eight different curves, from bottom to top, correspond to shells of size $(2^{-(i+1)/2}, 2^{-i/2})$ with $i = 6$–13. We clearly observe a common envelope to the $\Lambda(k)$ curves. Hence, the motion is clearly chaotic. Note that for this time

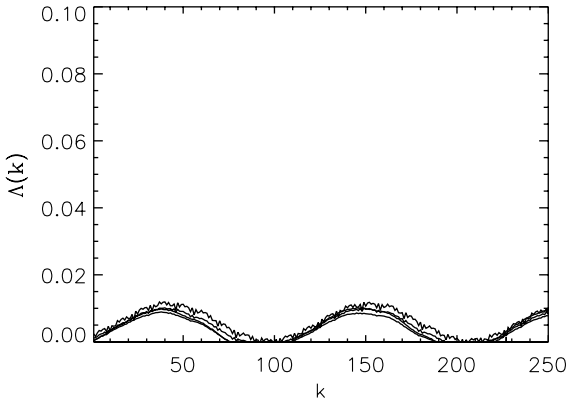

Fig. 3. The $\Lambda(k)$ curves for the time series of Fig. 1(c). Four different shells are used. The embedding parameters are $m = 4$ and $L = 1$. The computation is based on 1000 points.

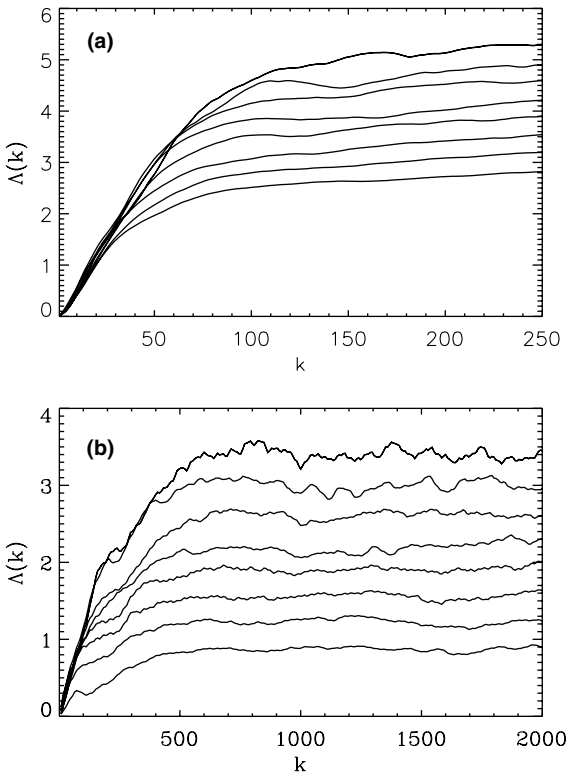

Fig. 4. (a) and (b) The $\Lambda(k)$ curves for the time series of Fig. 1(b) and (d). The embedding parameters (m, L) are $(4, 1)$ for (a) and $(24, 1)$ for (b). Respectively, 2000 and 3000 points are used in (a) and (b). The different curves in both figures, from bottom to top, correspond to shells of size $(2^{-(i+1)/2}, 2^{-i/2})$ with $i = 6$–13 for (a) and $i = 8$–15 for (b).

series, so long as the embedding dimension is larger than 2, the $\Lambda(k)$ curves always behave similarly to that shown in Fig. 4(a). However, when only a few hundred points are used, then the $\Lambda(k)$ curves are less smooth, especially when the evolution time is large. This is understandable, since the "diameter" of the attractor is then less well represented by too few points. Instead of showing such an example, we turn to study a short time series of 3000 points of Fig. 1(b) in Fig. 4(b). Note 3000 points has to be considered short here, since this means there are less than 400 points for each chaotic island. Nevertheless, we still clearly observe a common envelope to the $\Lambda(k)$ curves in Fig. 4(b).

We note that the common envelope may be broken down loose or be destroyed if one adds increasing amount of noise. When the number of points used in the computation is large, then we can quantitatively analyze how this happens. However, if one can only access to a very short time series data, which is typical for the study of population fluctuations, then such a quantitative analysis is no longer feasible. For this reason, we do not include any relevant results here. Instead, we refer interested readers to Gao [19] and Gao et al. [18,22,23].

Before we leave this section, we note three interesting features. First, the slope of Fig. 4(b) is considerably smaller than that of Fig. 4(a). This can be readily explained if one notices that the sampling time for $\{y_n, n = 1, 2, \ldots\}$ is 1, while that for $\{y_n^{(R)},\ n = 1, 2, \ldots\}$ is 8. Second, in order to obtain the result of Fig. 4(b), a very large embedding dimension of 24 is used. In pondering why prediction method fails to characterize the time series from the global attractor, Sugihara and May [9] surmised that maybe one has to choose the embedding parameters, especially the delay time, carefully. Their intuition is essentially correct, except that it is not the delay time but the embedding dimension. The reason for this is again that the sizes of the eight chaotic islands are very different. In order to simultaneously take into account all these different sized chaotic islands, one has to use a very large embedding dimension. Third, the amount that nearby orbits can diverge in $\{y_n, n = 1, 2, \ldots\}$ is considerably smaller than that in $\{y_n^{(R)},\ n = 1, 2, \ldots\}$. This is confirmed by noticing that the shells for Fig. 4(b) are $(2^{-(i+1)/2}, 2^{-i/2})$, with $i = 8$–15, thus smaller than that for Fig. 4(a). However, the flat parts of the $\Lambda(k)$ in Fig. 4(b) are lower than those in Fig. 4(a). On the other hand, the size of the attractor for Fig. 4(a) is about $1 \cdot \sqrt{m} = 2$, while that for Fig. 4(b) is $1 \cdot \sqrt{m} \approx 5$, where 1 is the range of the time series. (Recall that the time series is first normalized to the unit interval.) This feature is also easy to understand. For the $\{y_n, n = 1, 2, \ldots\}$ time series, the divergence is up to the size of the largest chaotic island, which is anyway small compared to the global attractor. For the $\{y_n^{(R)},\ n = 1, 2, \ldots\}$, the divergence can extend to the whole range within that island.

4. Diffusions on a torus

From an operational point of view, we can always try to compute a set of $\Lambda(k)$ curves for any type of signal, including the noisy oscillatory signals generated from the noisy population model studied here. Although the $\Lambda(k)$ curves corresponding to small shells are always positive, the linearly increasing parts of those curves do not form a common envelope. Hence, we have to conclude that the signal is not chaotic. More interestingly, the $\Lambda(k)$ curves for large evolution time k keep increasing when k increases. This motivates us to examine how nearby orbits diverge with the increase of the evolution time k. Specifically, we check whether the following power-law relation holds:

$$\langle \|X_{i+k} - X_{j+k}\| \rangle \sim k^{\alpha}, \tag{3}$$

where α is called the diffusion exponent. Related to stochastic oscillatory motions, three different types of diffusions have been observed [18,19]:

1. $\alpha > 1/2$: anomalous diffusion;
2. $\alpha = 1/2$: normal diffusion, similar to the standard Brownian motions;
3. $\alpha < 1/2$: subdiffusion.

Experimental data falling into this category include an oscillatory fluctuating velocity signal measured in a near wake behind a circular cylinder [19] and pathological tremors including essential tremor and tremor in the Parkinson's disease [21]. The two upper smooth curves (corresponding to two different shells) in Fig. 5 show the variation of $\langle \|X_{i+k} - X_{j+k}\| \rangle$ vs. k (in log–log scale) for the noisy version of the signal shown in Fig. 1(d), with the σ for the noise being 0.00001. A total of 5000 points are used in the computation. It can be easily found that the diffusion exponent α here is around 0.4, hence this is subdiffusion. Subdiffusions may be caused by a combination of very weak convergent flow around the limit cycle but very strong convergent flow away from the limit cycle [18]. Interestingly, the two smooth curves shown in Fig. 5 are island-independent. In other words, using the time series obtained from any of the eight islands, the results are always the same. However, when fewer points are used in the computation, the curves become less smooth. Instead of showing such an example, we show a $\langle \|X_{i+k} - X_{j+k}\| \rangle$ vs. k curve calculated from the original y-component of the time series, with only 3000 points. Now we observe a much less smooth curve. Nevertheless, the characteristic diffusional feature can still be clearly seen.

We should emphasize here that the two smooth curves in Fig. 5 characterize diffusions near a limit cycle. However, the very jagged curve in Fig. 5 really describes the diffusion on the torus. It just so happens that along the direction of the periodic transitions between the eight islands, the motion is precise, hence there is no diffusion. Within each island,

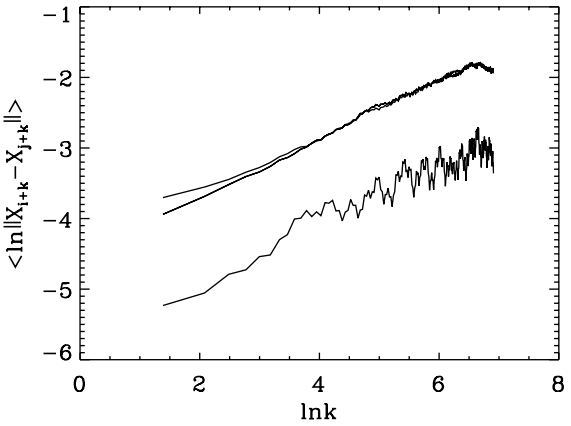

Fig. 5. (a) and (b) Log–log plot of the displacement curves for the time series of the noisy map when $r = 117$. The two upper more smooth curves are computed from the y-component of the island located at the lower right corner of the figure, with embedding parameters $(m, L) = (8, 1)$ and 5000 points. Two curves are plotted, corresponding to two different shells. The lower less smooth curve is computed from the y-component of the entire attractor, with $(m, L) = (12, 1)$ and 3000 points. The curve is arbitrarily shifted downward so that it can be easily distinguished from the upper two more smooth curves.

there is diffusion. For this reason, we term the overall diffusion an asymmetric diffusion wandering along the quasi-periodic orbit.

Before ending this section, we point out that when examining long-term diffusional features of a time series, it is not necessary to compute a series of $\langle \|X_{i+k} - X_{j+k}\| \rangle$ vs. k curves corresponding to different shells. This is because when k is reasonably large, all such curves will collapse together, as we have seen from the two upper smooth curves in Fig. 5.

5. Concluding remarks

In this paper, by studying a noisy population model, we have shown how quasi-periodic and chaotic dynamics can be readily characterized by computing a series of $\Lambda(k)$ curves corresponding to different scales in the reconstructed phase space. We have emphasized the importance of the existence of a common envelope to the $\Lambda(k)$ curves. That is the key to distinguish between true chaos and randomness. We have also shown that noisy oscillatory motions can be conveniently characterized by a diffusional scaling law. Due to the existence of population cycles, the diffusional scaling law may be especially relevant to the study of population fluctuations.

As we have pointed out in the end of last section, the diffusions observed here should be termed asymmetric diffusions on a torus. Those diffusions are somewhat degenerate, however. It would be every interesting to observe a genuine asymmetric diffusion on a torus, where along one direction of the oscillation, the diffusion is characterized by one non-zero diffusion exponent, while along the other direction of the oscillation, the diffusion is characterized by another non-zero exponent.

References

[1] Bjornstad ON, Grenfell BT. Science 2001;293:638.
[2] Hastings A, Hom CL, Ellner S, Turchin P, Godfray HCJ. Ann Rev Ecol Systemat 1993;24:1.
[3] Rand DA, Wilson HB. Proc Roy Soc Lond Ser B 1991;246:179.
[4] Costantino RF, Cushing JM, Dennis B, Desharnais RA. Nature 1995;375:227.
[5] Rohani P, Miramontes O. J Animal Ecol 1996;65:847.
[6] Cazelles B, Ferriere RH. Nature 1992;355:25.
[7] Barahona M, Poon CS. Nature 1996;381:215.
[8] Sugihara G, May RM. Nature 1990;344:734.
[9] Sugihara G, May RM. Nature 1992;355:26.
[10] Billings L, Schwartz IB. J Math Biol 2002;44:31;
Billings L, Bolt EM, Schwartz IB. Phys Rev Lett 2002;88:234101-1.

[11] Ott E. Chaos in dynamical systems. Cambridge University Press; 2002.
[12] Ruelle D, Takens F. Commun Math Phys 1971;20:167.
[13] Packard NH, Crutchfield JP, Farmer JD, Shaw RS. Phys Rev Lett 1980;45:712.
[14] Takens F. In: Rand DA, Young LS, editors. Dynamical systems and turbulence. Lecture notes in mathematics, vol. 898. Springer-Verlag, Berlin; 1981. p. 366.
[15] Sauer T, Yorke JA, Casdagli M. J Stat Phys 1991;65:579.
[16] Gao JB, Zheng ZM. Europhys Lett 1994;25:485.
[17] Gao JB, Zheng ZM. Phys Rev E 1994;49:3807.
[18] Gao JB, Chen CC, Hwang SK, Liu JM. Int J Mod Phys B 1999;13:3283.
[19] Gao JB. Physica D 1997;106:49.
[20] Wolf A, Swift JB, Swinney HL, Vastano JA. Physica D 1985;16:285.
[21] Gao JB, Tung WW. Pathological tremors as diffusional processes. Bio Cybern 2002;86:263.
[22] Gao JB, Hwang SK, Liu JM. Phys Rev A 1999;59:1582;
Phys Rev Lett 1999;82:1132.
[23] Hwang K, Gao JB, Liu JM. Phys Rev E 2000;61:5162.